Unprecedented coupling of natural rubber and ELP: synthesis, characterization and self-assembly properties

Tingting Zhang, Frédéric Peruch, Anne-Laure Wirotius, Emmanuel Ibarboure, Frédéric Rosu, Christophe Schatz, Bertrand Garbay

▶ **To cite this version:**

Tingting Zhang, Frédéric Peruch, Anne-Laure Wirotius, Emmanuel Ibarboure, Frédéric Rosu, et al.. Unprecedented coupling of natural rubber and ELP: synthesis, characterization and self-assembly properties. Polymer Chemistry, 2021, 12 (41), pp.6030-6039. 10.1039/d1py00969a . hal-03403619

HAL Id: hal-03403619
https://hal.science/hal-03403619

Submitted on 15 Nov 2021

HAL is a multi-disciplinary open access archive for the deposit and dissemination of scientific research documents, whether they are published or not. The documents may come from teaching and research institutions in France or abroad, or from public or private research centers.

L'archive ouverte pluridisciplinaire **HAL**, est destinée au dépôt et à la diffusion de documents scientifiques de niveau recherche, publiés ou non, émanant des établissements d'enseignement et de recherche français ou étrangers, des laboratoires publics ou privés.

Distributed under a Creative Commons Attribution - NonCommercial - NoDerivatives 4.0 International License

Unprecedented coupling of natural rubber and ELP: synthesis, characterization and self-assembly properties†

Tingting Zhang,[a] Frédéric Peruch, *[a] Anne-Laure Wirotius,[a] Emmanuel Ibarboure,[a] Frédéric Rosu,[b] Christophe Schatz[a] and Bertrand Garbay *[a]

Developing new biomaterials is an active research area owing to their applications in regenerative medicine, tissue engineering and drug delivery. Di-block copolymers, combining a hydrophobic block with a hydrophilic one, are good candidates to develop biomaterials, but they are often obtained with non-bio-derived components. To circumvent this issue, we used two biocompatible blocks: a hydrophobic block made of polyisoprene (PI) extracted from natural rubber, and a hydrophilic block consisting in recombinant elastin-like polypeptide (ELP). We report the synthesis and characterization of the polyisoprene-*block*-ELP copolymers, coupled *via* Michael addition between the double bond of the maleimide previously grafted onto the PI, and the thiol function of the C-terminal cysteine of the ELP. The resulting conjugate can self-assemble into well-defined nanoparticles of hydrodynamic radius of 35–45 nm in aqueous solution. These nanoparticles can encapsulate hydrophobic molecules, and therefore could be used as drug delivery systems for various hydrophobic drugs.

Introduction

Polypeptides are of great interest for biomedical applications such as drug delivery and tissue engineering because they are biodegradable and biocompatible.[1,2] Hybrid block copolymers containing a polypeptide block and a non-polypeptide block are of interest since they can combine the intrinsic properties of polypeptide and the physico-chemical properties of the second block which could bring solubility, elasticity, strength, *etc.* Of particular interest, polypeptide-*block*-polyisoprene copolymers can mimic the natural rubber (NR), which is composed of 1,4-*cis* polyisoprene (PI) and a small amount of proteins that are believed to play an important role in the physical properties of NR.[3–5] In addition, PI is enzymatically degradable[6] and biocompatible.

Polypeptide-*block*-PI copolymers can be obtained by ring opening polymerization of the *N*-carboxyanhydride of the selected amino acid using the PI as a macroinitiator. This approach was successfully used to synthesize poly(γ-benzyl-L-glutamate),[7,8] poly(L-lysine),[9] and poly(ε-*tert*-butyloxycarbonyl-L-lysine[8] onto polyisoprene. However, a limitation of this approach is that the polypeptide blocks were always based on a single amino acid, which is obviously not representative of the complex protein structures. In addition, the molar-mass dispersity of the polypeptide block is not negligible unlike natural proteins.

Our goal was to synthesize a diblock polymer combining PI with a recombinantly produced elastin-like polypeptide (ELP). ELPs are synthetic polypeptides bio-inspired from the hydrophobic region of tropoelastin.[10] They consist of multiple repeats of Val-Pro-Gly-Xaa-Gly pentapeptides, where the guest residue (Xaa) can be any natural amino acid except proline. ELPs are characterized by their thermosensitivity, being soluble in water below a transition temperature (T_t), which corresponds to the cloud point temperature, and becoming insoluble when heated above this T_t.[11,12] T_t depends on the chain length, on the nature of the guest residue Xaa (*e.g.* polar, charged, hydrophobic), on the polypeptide concentration, and on the presence of salts.[13] Recombinantly produced ELP are often preferred, because they have controlled sequence and can have high molecular mass contrarily to those chemically synthesized.[14]

To solve solubility issues between the hydrophobic PI and the hydrophilic ELP blocks we used a PI block of relatively low molar mass, *i.e.*, below 10 000 g mol^{-1}. On the other hand, we selected from our library a rather hydrophobic ELP block based on the Grand Average of Hydropathy (GRAVY) index, which is calculated as the sum of hydropathy values of all the amino acids, divided by the number of residues in the sequence.[15] Negative GRAVY value indicates that the protein is

[a]*Univ. Bordeaux, CNRS, Bordeaux INP, LCPO, UMR 5629, F-33600 Pessac, France. E-mail: bertrand.garbay@bordeaux-inp.fr, frederic.peruch@enscbp.fr*
[b]*Univ. Bordeaux, CNRS & Inserm, IECB, UMS3033, US001, 33607 Pessac, France*
†Electronic supplementary information (ESI) available. See DOI: 10.1039/d1py00969a

non-polar, and positive value indicates that the protein is polar. We synthesized ELPs containing isoleucine (I) at the guest position of every VPGXG units.[16,17] The sequence of these ELPs is MW(VPGIG)$_n$C, with n = 20, 40 and 60. Their molar masses vary from 8.9 to 25.9 kg mol^{-1}, and their GRAVY index is 1.26. Among these ELPs, we selected the shortest one, MW(VPGIG)$_{20}$C, referred as I20, because (i) it can be produced in higher yields than the larger ones, (ii) it has a lower tendency to aggregation than the 40 and 60 pentamers, (iii) the size of the I20 (8.9 kDa) is closer to that of the PI used, and therefore the final diblock is expected to have a rather balanced hydrophobic/hydrophilic mass ratio of approximately 0.7. In addition, the I20 block has one cysteine residue at the C-terminal position that will be conveniently used for the coupling reaction with one PI block.

In this work, the synthesis, purification and characterization of the I20-*b*-PI copolymer are described. The self-assembly properties and the possibility to encapsulate hydrophobic molecules are investigated as well.

Experimental

Materials

Natural rubber (NR) PB235 was kindly provided by UMR iATE in Thailand. 3-Chloroperoxybenzoic acid (*m*CPBA) (70–75%, Acros), periodic acid (H_5IO_6) (≥99%, Aldrich), acetic acid (99%, Aldrich), sodium triacetoxyborohydride ($NaBH(OAc)_3$) (97%, Aldrich), Na_2CO_3 (>99.5%, Sigma-Aldrich), KOH (85%), 6-maleimidohexanoic acid (>90%, Sigma-Aldrich), oxalyl chloride (≥99%, Sigma-Aldrich), Tris(2-carboxyethyl)phosphine hydrochloride (TCEP. HCl) (Sigma-Aldrich), NaCl (Sigma-Aldrich), DMSO (Sigma-Aldrich), PBS 10× (Eurobio), pyrene (98%, Alfa Aesar), osmium tetroxide (Delta microscopy), and Nile Red (Carl Roth) were used without further purification. Celite® was purchased from Sigma-Aldrich. Tetrahydrofuran (THF), dimethylformamide (DMF), and dichloromethane (DCM) were purified using the PureSolv MD7 system from INERT. Triethylamine (TEA) (99% Acros organics) was dried using CaH_2 and distilled prior to use. Chloroform (VWR chemicals), methanol, ethanol and diethyl ether (reagent grade, Aldrich) were used as received. Laemmli Sample Buffer, Tris/glycine/SDS buffer (TGS buffer), Precision Plus Protein™ Unstained Standards, and 4–20% Mini-PROTEAN™ TGX Stain-Free™ polyacrylamide gels were purchased from BioRad. InstantBlue® Coomassie protein stain was from Sigma-Aldrich. Ultrapure water (18 MΩ cm) was obtained by passing in-house deionized water through a Millipore Milli-Q Biocel A10 purification unit. Bacto Tryptone (Sigma), Yeast extract (Sigma), Ampicillin (Sigma) and isopropyl β-D-thiogalactopyranoside (IPTG, VWR chemicals) were used for cell culture.

Production and purification of I20

Production and purification of ELP I20 was performed as already described.[17] Briefly, a single bacterial colony was cultured overnight at 37 °C in a rotary shaker at 200 rpm in 50 mL of lysogeny broth (LB) medium (1% bacto tryptone, 1% yeast extract, 0.5% NaCl) containing 100 μg mL^{-1} ampicillin. Thereafter, this seed culture was inoculated into 0.95 L of LB medium supplemented with glucose (1 g L^{-1}) and ampicillin (100 μg mL^{-1}), and cells were cultivated at 37 °C. When the $OD_{600\ nm}$ reached a value close to 0.8, isopropyl β-D-thiogalactopyranoside (IPTG) was added to a final concentration of 0.5 mM, and temperature of the incubator was decreased to 25 °C. After 12 h the culture was harvested by centrifugation at 6000*g* and 4 °C for 15 min, and the cell pellet was suspended with 10 mL g^{-1} wet weight in phosphate buffered saline (PBS) buffer. Thereafter cells were lyzed by sonication, and the insoluble debris were removed by centrifugation at 10 000*g* and 4 °C for 30 min. The cleared lysate was subjected to three successive cycles of Inverse Transition Cycling (ITC).[18] Briefly, ELP was precipitated at 30 °C and centrifuged at 10 000*g* and 25 °C for 30 min ("warm spin"). The ELP-containing pellets were dissolved in cold water and the insoluble proteins were eliminated by centrifugation for 15 min at 10 000*g* and 4 °C ("cold spin"). The protein content of the purified ELP I20 solutions was measured by spectrophotometry at 280 nm with a NanoDrop 1000 (ThermoScientific). Finally, the purified I20 was dialyzed against ultrapure water at 4 °C (Spectra Por7, MWCO1000, Spectrum Laboratories), and then lyophilized.

For SDS-PAGE analyses, polypeptide-containing samples were mixed with the loading buffer and loaded onto 4–20% gradient acrylamide gels (BioRad). Electrophoreses were performed in TGS buffer (25 mM Tris, 192 mM glycine, 0.1% SDS, pH 8.6). After migration, protein bands were revealed by the stain-free method using a Gel Doc apparatus (Biorad). Gels were also subsequently stained with InstantBlue® Coomassie protein stain. Densitometric analyses were performed with the Image Lab software (BioRad).

Synthesis of maleimide end-functionalized PI

Synthesis of heterotelechelic keto/aldehyde PI (PIEG). This reaction was performed as already described.[8] Briefly, 10 g of NR were cut into small pieces and dissolved overnight at RT in 500 mL of THF in round-bottom flask under stirring. In parallel, 550 mg (3.2 mmol) of *m*CPBA were dissolved in 50 mL of THF, and then added dropwise into the NR solution to epoxidize the PI. After 2 h, a solution of 1.5 g of periodic acid (2 eq. relative to *m*CPBA, 6.5 mmol) in 50 mL of THF was added dropwise to the epoxidized NR solution. The reaction was carried out for 2 hours, and then 2 g of Na_2CO_3 were added and stirred for 15 min to neutralize acids. The reaction mixture was filtered on glass filter with Celite®, concentrated using a rotary evaporator, and precipitated into a large excess of cold ethanol containing KOH (5.9 mM). The precipitated polymer was then solubilized in 50 mL of diethyl ether and filtered again on Celite®. The purified product was dried overnight at 40 °C under dynamic vacuum. This heterotelechelic keto/aldehyde PI was named PIEG and was obtained as yellowish and transparent viscous liquid. Yield: 70%, M_n = 5500 g mol^{-1}, D = 1.57. ^{1}H NMR (400 MHz, $CDCl_3$) δ (ppm): 9.77 (t, 1H, $-CH_2CHO$), 5.12 (t (broad), 80H, $-CH_2CH=$), 2.48 (t, 2H,

–CH_2CHO), 2.43 (t, 2H, –CH_2COCH_3), 2.34 (t, 2H, –CH_2CH_2CHO), 2.04 (m (broad), 316H, –CH_2CH= and –$CH_2C(CH_3)$=), 1.68 (s (broad), 240H, –(CH_3)C=CH–). ^{1}H NMR spectrum and size exclusion chromatogram are shown in ESI Fig. S1 and S2.†

Synthesis of heterotelechelic keto/hydroxyl PI (PI–OH). This reaction was performed under argon atmosphere as already described.[8] Briefly, 6 g of purified PIEG 5500 g mol^{-1} (equivalent to 1.2 mmol of aldehyde groups) were dissolved in 25 mL of dry THF. Then, 1.02 g (4.8 mmol, 4 eq.) of $NaBH(OAc)_3$ and 76 μL (1.2 mmol, 1 eq.) of acetic acid were added to the reaction. The mixture was stirred at 40 °C overnight. The product was then precipitated twice with large excess of cold methanol, solubilized in 50 mL of Et_2O, filtered on a glass filter with Celite® and dried overnight at 40 °C under dynamic vacuum. Yield: 80%, M_n = 5500 g mol^{-1}, D = 1.56. ^{1}H NMR ($CDCl_3$) δ (ppm): 5.12 (t (broad), 80H, –CH_2CH=), 3.63 (t, 2H, –CH_2OH), 2.43 (t, 2H, –$CH_2(CO)CH_3$), 2.04 (m (broad), 316H, –CH_2CH= and –$CH_2C(CH_3)$=), 1.68 (s (broad), 240H, –(CH_3)C=CH–). ^{1}H NMR spectrum is shown in Fig. S3.†

Synthesis of maleimidohexanoic chloride. This reaction was performed under argon atmosphere. 2.75 g (12 mmol) of maleimidohexanoic acid were solubilized in 15 mL of dry dichloromethane (DCM). 2.25 mL (26 mmol, ~2 eq.) of oxalyl chloride, and 150 μL of *N*,*N*-dimethylformamide (DMF) were added to the solution, and incubated for 1 hour at room temperature. Then, oxalyl chloride and DCM in excess were removed under dynamic vacuum by an overnight incubation at room temperature. Yield: 100%. ^{1}H NMR (Fig. S4†) ($CDCl_3$) δ (ppm): 6.69 (s, 2H, –CH=CH–), 3.52 (m, 2H, –CH_2N=), 2.88 (m, 2H, –$CH_2(CO)Cl$), 1.73 (m, 2H, –$CH_2CH_2(CO)Cl$), 1.62 (m, 2H, –CH_2CH_2N=), 1.34 (m, 2H, –$CH_2CH_2CH_2(CO)Cl$).

Synthesis of *N*-polyisoprene-maleimide (PIMAL). This reaction was performed under argon atmosphere. A mixture of 2 mL of dry TEA (14 mmol, 40 eq.) and 8 mL of anhydrous THF containing 1 g of maleimidohexanoic chloride (4.3 mmol, 10 eq.) was slowly added to a solution of 8 mL of dry THF containing 2 g of PIOH (containing 0.36 mmol of OH group). The reaction was done for 4 h at 25 °C. The product of the reaction was separated by two successive precipitations into a large excess of cold methanol, then dissolved in Et_2O, filtered on a glass filter with Celite®, concentrated using a rotary evaporator, and dried overnight at room temperature under dynamic vacuum. Yield: 90%, M_n = 5500 g mol^{-1}, D = 1.64. ^{1}H NMR ($CDCl_3$) δ (ppm): 6.67 (s, 2H, –CH=CH–), 5.12 (t (broad), 80H, –CH_2CH=), 4.00 (t, 2H, –CH_2OCO–), 3.5 (t, 2H, –CH_2N), 2.43 (t, 2H, –CH_2COCH_3), 2.27 (t, 2H, –$CH_2(CO)O$–), 2.04 (m (broad), 316H, –CH_2CH= and –$CH_2C(CH_3)$=), 1.68 (s (broad), 240H, –(CH_3)C=CH–). IR-FT: stretching vibration of =C–H (3036 cm^{-1}), –CH_3 (2960 cm^{-1}), –CH_2– (2914 cm^{-1}, 2853 cm^{-1}), –CO– (1720 cm^{-1} which was overlapped with CO of maleimide), C=C (1665 cm^{-1}), –C–H deformation from –CH_2 (1446 cm^{-1}) and –CH_3 (1375 cm^{-1}), =C–H wagging at 828 cm^{-1} and –CH_2 rocking at 740 cm^{-1} from PI backbone. The stretching vibration of CO (1711 cm^{-1}), wagging of =CH (833 cm^{-1} which is overlapped with =C–H waging of PI) and deformation vibration of –C–H of *cis* R_1CH=CHR_2 (696 cm^{-1}) from maleimide. ^{1}H NMR spectrum is shown in Fig. S5,† and IR spectrum in Fig. S6.†

Synthesis and purification of the I20-*block*-PI copolymer (I20-*b*-PI). 2 mL of an aqueous solution of ELP I20 (8 mg mL^{-1}, 1.8 μmol) was incubated for 3 h at 4 °C with 100 μL of Tris(2-carboxyethyl) phosphine hydrochloride (TCEP) 1 M to reduce the intermolecular disulfide bridges. The reduced I20 was recovered by an ITC cycle, dried under dynamic vacuum for 1 h, and then dissolved in 450 μL of a 2 : 1 (v/v) mixture of chloroform and methanol. After this solubilization step, 300 μL of chloroform were added to the glass vial to increase the chloroform/methanol ratio to 4 : 1 (v/v), and the solution was further incubated under magnetic stirring for 1 h at room temperature. In parallel, 50 mg (9 mmol) of PIMAL 5500 g mol^{-1} were solubilized in 800 μL of chloroform. After 1 h of incubation, 200 μL of methanol were added to obtain a final chloroform–methanol ratio of 4 : 1 (v/v). Finally, the two solutions containing the solubilized ELP and PIMAL were mixed, and 100 μL of TEA (0.46 M) was added. The reaction mixture containing 1.8 μmol of ELP and 9 μmol of PIMAL was stirred at room temperature for 24 h. A sample of 50 μL was then pipetted out, dried, and solubilized in SDS-PAGE loading buffer (BioRad) for analysis. After the reaction, the chloroform–methanol mixture was evaporated, and the dry residues were washed three times for 3 h under magnetic stirring with THF to eliminate the unreacted PIMAL. The supernatants were analyzed by NMR to check their content in PIMAL. To extract the unreacted I20, dried residues were then incubated with 1 mL of 70% ethanol for 24 h at 4 °C under magnetic agitation, centrifuged at 10 000*g* for 30 min at 4 °C, and the supernatant containing the I20 was eliminated. The pellet enriched in I20-*b*-PI was kept for further analyses. All these purification steps were monitored by SDS-PAGE analyses.

Self-assembly of I20-*block*-PI copolymer in aqueous solution

5 mg of I20-*b*-PI were dissolved in 1 mL of a 1 : 4 (v/v) mixture of DMF/THF and filtered through 0.45 μm pore size PTFE membrane. The block copolymer was nanoprecipitated by adding 1.5 mL of milliQ water in 200 μL of I20-*b*-PI solution under stirring at room temperature using a syringe pump R-99 E (RAZEL™) at a flow rate of 100 μL min^{-1}. The final polymer concentration was 0.27 mg mL^{-1}. The organic solvent was removed from the particle dispersion by two successive dialysis steps of 24 h against 2 L of deionized water.

Methods

The molar masses of polymers were determined by size exclusion chromatography (SEC) using an Ultimate 3000 system from Thermoscientific equipped with a diode array detector. The system was also equipped with a multi-angle light scattering detector and a differential refractive index detector from Wyatt technology. Polymers were separated on two Shodex Asahipack gel columns GF310 and GF510 (300 × 7.5 mm) (exclusion limits from 500 g mol^{-1} to 300 000 g mol^{-1}) using DMF and lithium bromide (1 g L^{-1}) at 50 °C as eluent at a flow

rate of 0.5 mL min^{-1}. The dn/dc value for I20-*b*-PI was determined as 0.13 mL g^{-1} using the differential refractive index detector of the SEC. An Easyvial kit of polystyrene from Agilent was used as standards (M_n from 162 to 364 000 g mol^{-1}) to calibrate the column. Fourier transform infrared spectroscopy (FT-IR) spectra of the polymer powders were acquired between 4000 and 400 cm^{-1} in attenuated total reflectance (ATR) mode with a Bruker Vertex 70 instrument equipped with a GladiATR diamond. ^{1}H, DOSY, HSQC and HMBC NMR spectra were recorded in $CDCl_3$ at 298 K on a Bruker Avance NEO spectrometer operating at 400.3 MHz. All DOSY (diffusion ordered spectroscopy) measurements were performed with a 5 mm Bruker multinuclear *z*-gradient direct cryoprobe-head capable of producing gradients in the *z* direction with strength 53.5 G cm^{-1}. Each sample was dissolved in 0.4 mL of $CDCl_3$ for internal lock and spinning was used to minimize convection effects. The DOSY spectra were acquired with the ledbpgp2s pulse program from Bruker topspin software. The duration of the pulse gradients and the diffusion time were adjusted to obtain full attenuation of the signals at 95% of maximum gradient strength. The values were 5.0 ms for the duration of the gradient pulses and 300 ms for the diffusion time. The gradients strength was linearly incremented in 16 steps from 5% to 95% of the maximum gradient strength. A delay of 5 s between echoes was used. The data were processed using 8192 points in the F2 dimension and 128 points in the F1 dimension with the Bruker topspin software. Field gradient calibration was accomplished at 25 °C using the self-diffusion coefficient of $H_2O + D_2O$ at 19.0×10^{-10} m^2 s^{-1}.

Circular dichroism spectra were recorded on a Jasco J-1500 equipped with a Peltier temperature control accessory (JASCO, Hachioji, Japan). Each spectrum was obtained by averaging two scans collected at 50 nm min^{-1}. The CD spectrum of pure water solution was subtracted from the average scan for each sample.

The critical aggregation concentration (CAC) of the copolymer in aqueous solution was determined as previously described.[19,20] Briefly, solutions of I20-*b*-PI in deionized water with concentrations varying from 10^{-6} mg mL^{-1} to 2×10^{-1} mg mL^{-1} were prepared. Then, 1 µL of pyrene solution at 1 mg mL^{-1} in THF was added into 500 µL of particle dispersion prepared at various concentrations and incubated under stirring at 300 rpm for 10 h at room temperature. The dispersions were characterized by fluorescence spectroscopy using a Jasco FP 8500 spectrofuoromete. The excitation wavelength was set at 319 nm, and the fluorescence emission of pyrene was recorded between 360 and 400 nm. The intensities of the first ($I1$) and third ($I3$) vibrionic band of pyrene were determined at 373 nm and 385 nm respectively. The $I1/I3$ ratio was plotted as function of the polymer concentration. The CAC was determined from the onset of the decrease in $I1/I3$.

Dynamic light scattering (DLS) analysis of the suspension of PI-*b*-ELP nanoparticles was performed at 25 °C by using a Nano ZS instrument (Malvern U.K.) working at a 90° angle detection. The hydrodynamic radius (R_h) and the polydispersity index (PDI) were calculated from autocorrelation functions using the cumulant method. The derived count rate (DCR) was defined as the mean scattered intensity normalized by the attenuation factor. The zeta potential was measured with the same apparatus using the M3-PALS technique.

For transmission electron microscopy (TEM) analyses, 20 µL of the polymer dispersion at 0.27 mg mL^{-1} were deposited onto lacey carbon grids, and then water was evaporated at room temperature. The grid was incubated with vapor of osmium tetroxide (OsO_4, 4% in aqueous solution) for 12 h at room temperature. TEM analyses were performed at 80 kV acceleration voltage with a Hitachi H7650 microscope equipped with an Orius camera (Gatan, Paris, France). Pictures were acquired with the digital micrograph software.

Adsorbed structures at the solid/solution interface were examined using a NanoScope IIIa Multimode atomic force microscope (Digital Instruments, CA) in Contact Mode, equipped with a standard fluid cell. Standard cantilevers were used with sharpened Si3N4 tips. These were irradiated with ultraviolet light for 30 min prior to use. The solution was held in a Plexiglas fluid cell, sealed by a silicone O-ring and resting on a muscovite mica substrate. The cell and the cantilever were cleaned by sonication for 30 min in deionized water at 40 °C and then dried using filtered nitrogen prior to use. The mica substrate was cleaved using adhesive tape and immediately used, to avoid contamination by ambient dust particles or volatile molecules. The cell was completely filled with about 0.5 mL of the nanoparticles solution at a concentration of 0.27 mg mL^{-1}. Before imaging the surfaces, the polymer was allowed to adsorb onto mica during at least 12 h.

Encapsulation of Nile red was as follows: 2 µL of Nile red at 1 mg mL^{-1} in DMSO were added in 600 µL of a solution of I20-*b*-PI nanoparticles at 0.27 mg mL^{-1}. The solution was incubated under stirring for 24 h at room temperature. The fluorescence emission spectrum of the Nile red-loaded particles was recorded between 587 and 800 nm (λ_{ex} = 570 nm) with a Jasco FP 8500 spectrofluorometer, and compared to the spectrum obtained with a solution of Nile red in water. Nile red release was studied by placing loaded nanoparticles (600 µL at 0.27 mg mL^{-1}) into a dialysis device Spectra-Por® Float-A-Lyzer® G2 (3.5–5 kDa MWCO). The device was then placed in 1 L of water, and incubated at room temperature in the dark under magnetic stirring. After excitation at 570 nm the fluorescence of the dialyzed sample was measured between 587 nm and 800 nm. The experiment was performed in triplicate and the data was presented as mean ± SD.

Results and discussion

Synthesis and purification of I20-*b*-PI

Our goal was to graft a low MW PI block in the 5 to 10 kg mol^{-1} range to the N-terminal cysteine of the I20 ELP to obtain an amphiphilic diblock copolymer structure. The different steps of the synthesis process are depicted in the Scheme 1.

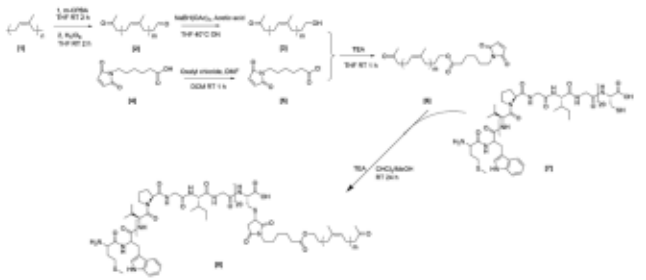

Scheme 1 Synthesis of I20-*b*-PI. Five main steps were used. 1: Epoxidation and controlled hydrolysis of natural rubber to obtain keto/aldehyde PI (PIEG); 2: reduction of the aldehyde ends of PIEG to obtain keto/hydroxyl PI (PIOH); 3: conversion of maleimidohexanoic acid (MalOH) to an acid chloride form (MalCl); 4: grafting of the maleimide group on the PIOH to obtain – polyisoprene-maleimide (PIMAL); 5: Michael addition reaction between the maleimide group from PIMAL and the N-terminal cysteine residue of the ELP I20.

The synthesis, purification and characterization of the recombinant ELP I20 was reported in a previous work.[17] Briefly, production of the recombinant protein was performed by *E. coli* cells, and purification from the cell lysate was done using the ITC protocol.[18] We optimized the previously used ITC procedure, by lowering the temperature of the hot-spin step from 30 °C to 25 °C, and by solubilizing the corresponding hot-spin pellets in deionized water instead of salt-containing solutions. These changes led to a large increase in the yield of purified I20 from 32.7 ± 13.5 mg L^{-1} culture[17] to 243 ± 48 mg L^{-1} culture ($n = 4$).

The polyisoprene originally found in natural rubber (NR) is of high molar mass (>500 kg mol^{-1}), and to reduce it a partial epoxidation of NR by *m*-CPBA followed by cleavage with periodic acid of the formed epoxy units was carried out.[8,21] The final purified product heterotelechelic keto/aldehyde PI (PIEG) was characterized by ^{1}H NMR and size exclusion chromatography (SEC) (Fig. S1 and S2†). The ^{1}H NMR spectrum confirmed the presence of a peak at 9.77 ppm corresponding to the hydrogen of the aldehyde function, and another one at 2.48 ppm corresponding to the "–CH_2" group in α position of the aldehyde's carbonyl. Thank to NMR, the number-average molar mass ($\overline{M_n}$) was calculated to be around 5500 g mol^{-1}. The SEC trace of PIEG completely shifted to higher retention time when compared to the original NR one. Using PS standards calibration, the $\overline{M_n}$ of PIEG was evaluated to be 6900 g mol^{-1} and its dispersity (D) was 1.6. Thereafter, the aldehyde end group of PIEG was selectively reduced into a hydroxyl group using $NaBH(OAc)_3$. Heterotelechelic keto/hydroxyl PI (PI–OH) was obtained in good yield (80%) and its structure was confirmed by ^{1}H NMR spectrometry (Fig. S3†). Indeed, the peak corresponding to the aldehyde proton of PIEG at 9.77 ppm disappeared totally and a peak at 3.63 ppm was observed, corresponding to the "–CH_2" group in α position of the hydroxyl function.

In parallel, we synthesized maleimidohexanoic chloride by reacting maleimidohexanoic acid with oxalyl chloride. ^{1}H NMR spectrum of the product showed that protons from the "–CH_2" groups in α position of the carboxylic acid shifted from 2.30 ppm to 2.80 ppm, and the broad peak around 1.61 ppm splits into two distinct peaks at 1.72 (–CH_2CH_2(CO)Cl) and 1.60 ppm (–CH_2CH_2N=), confirming the identity of maleimidohexanoic chloride (Fig. S4†).

Consecutive reaction of PI–OH with maleimide acyl chloride to obtain PI bearing a maleimido group as a chain end was successfully performed with a final yield of 90%. The *N*-polyisoprene-maleimide (PIMAL) structure was then characterized. ^{1}H NMR spectrum (Fig. S5†) showed that the signal of the "–CH_2" group in α position of the hydroxyl, was totally shifted from 3.63 ppm (PIOH) to 4.03 ppm confirming the formation of the ester function. In addition, protons from the double bond of the maleimide group were visible at 6.67 ppm. Purified PIMAL was also analyzed with a Fourier Transform Infrared Spectrometer (FT-IR, Fig S6†). The purified PIMAL spectrum shows the presence of the stretching vibrations of –C–H from the PI backbone, and the bending vibration of –C–H of the *cis* double bond from the maleimide, confirming the grafting of the maleimide function at the end of the PI chains.

After the preparation of the two blocks, the challenge was to find a solvent, or a mixture of solvents able to solubilize both the hydrophobic PIMAL and the hydrophilic ELP. PIMAL solubility was assessed by simple visual inspection of polymer solutions prepared in various solvents at a concentration of 50 mg mL^{-1}. PIMAL was found to be soluble in chloroform, dichloromethane, tetrahydrofurane and hexafluoroisopropanol, but not in toluene, cyclohexane or methanol. The solubility of the polypeptide I20 was also evaluated in different solvents at a concentration of 16 mg mL^{-1}. After 48 h at RT under agitation, the solution was pipetted out, filtered through 0.4 μm nylon filter and the solvent evaporated. The dried residues were analyzed by gel electrophoresis to evaluate the protein content. A typical result is shown in Fig. S7.† I20 was not soluble in the solvents tested, albeit at a low level (~10% of total polypeptide) in chloroform. To go further, we looked at mixtures of solvents that were used to extract natural proteolipids from animal or plant tissues. Indeed, in mammals several proteolipids are particularly enriched in the myelin sheath of the central nervous system,[22,23] and they were efficiently extracted by mixtures of chloroform/methanol.[24] We therefore studied the solubility of PIMAL and I20 in different chloroform/methanol mixtures (1 : 1, 2 : 1 and 4 : 1, v/v) and found that a ratio of 4 : 1 was satisfactory for both macromolecules (Fig. S8†). I20 was almost fully soluble (>95% as estimated by densitometric analyzes of SDS-PAGE) in a chloroform/methanol mixture 4 : 1.

Before the coupling reaction, ELP I20 was reduced by TCEP treatment to cleave the intermolecular disulfide bridges that were formed between cysteine from two monomers, and therefore generate free thiols. After this treatment, only trace amounts of dimers remained in the sample (lane 1, Fig. 1A). The coupling of ELP I20 with the PI block was performed *via* a Michael addition involving the maleimide group end-grafted onto the PI and the thiol function of the C-terminal cysteine of

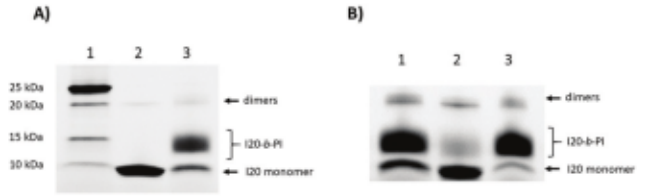

Fig. 1 SDS-PAGE analyses of the polypeptide I20 and of the copolymer I20-*b*-PI. (A) Analyses of the reaction product. (1) Molecular mass standard. (2) I20 ELP reduced by TCEP treatment. (3) Products obtained after 20 hours of reaction at room temperature. (B) Follow-up of the purification process. (1) Reaction products after the THF extraction to eliminate the excess of unreacted PIMAL. (2) Content of the supernatant from the ethanol wash at 4 °C. (3) Material that was not solubilized by cold ethanol.

the ELP (Scheme 1). The progress of the coupling reaction was monitored by SDS-PAGE analysis, because we hypothesized that the I20-*b*-PI copolymer has a lower electrophoretic mobility than that of I20. Fig. 1A shows a typical result obtained for a reaction performed for 20 hours at room temperature with 50 mg of PIMAL and 16 mg of ELP I20 (molar ratio 5 : 1).

After the coupling reaction (lane 3, Fig. 1A), we clearly see a decrease in the intensity of the band corresponding to the I20 monomer, and the appearance of a new band, the relative mobility of which, between 13 and 15 kg mol^{-1} by comparison with the protein standards, being between those of the I20 monomer (8.9 kg mol^{-1}) and dimer (17.8 kg mol^{-1}). We hypothesized that this new band corresponded to I20-*b*-PI. The fact that this band was slightly smearing can be explained by the dispersity of the PI block, so was the diblock. This apparent molecular mass is close to the 15 kg mol^{-1} expected after the coupling of the ~6 kg mol^{-1} PIMAL and the 8.9 kg mol^{-1} I20. Fig. 1A also shows that not all the I20 reacted during the incubation period, because some ELP monomers and dimers were still detected on the gel. Densitometric analyzes of the gel showed that the intensity of the I20-*b*-PI band represents around 60% of the total intensity measured in the corresponding lane. We therefore sought for improvements. We varied the amount of TEA, the PIMAL/I20 molar ratios, and the reaction time (Fig. S9†) but these optimization trials only marginally improved the yield of I20-*b*-PI, which levelled off around 65–70%. It was therefore necessary to purify the I20-*b*-PI. After the coupling reaction, chloroform/methanol was eliminated by evaporation and the dried residues were recovered. Un-reacted PIMAL was totally eliminated by three successive washes with THF, as showed by NMR analyses (Fig. S10†). The protein content of these THF extracts was analyzed by SDS-PAGE (Fig. S11†). This experiment demonstrates that neither the I20-*b*-PI, nor free I20, were solubilized during the THF extraction. The next step was to eliminate the ELP I20 that did not react with PIMAL. Our first attempts were made by incubating the THF-insoluble fraction with cold water, as it could have been hypothesized that the un-reacted I20 (monomers and dimers) would be solubilized in the cold water fraction, because their T_ts were around 20 °C,[16,17] and that the I20-*b*-PI diblock would not be solubilized because of its increased hydrophobicity. However, our results showed that this step was not as efficient as expected (Fig. S12†). Cold-water treatment allowed only partial extraction of the free I20 monomers, roughly 50% of the sample content. In addition, none of the I20 dimers were extracted using this protocol. It thus appeared that after the reaction and the different successive steps of washing and drying of the samples, a fraction of the I20 was not water-soluble at a temperature below its T_t. This could be the consequence of the THF washes, and drying steps that could have removed the water molecules closely linked to the polypeptide, and therefore preventing its further solubilization in water. A similar phenomenon has been reported for leucine-containing ELPs.[25] We therefore sought for other solvents, or mixtures of solvents, to remove ELP from the reaction mixture. We tested different HFIP/water and ethanol/water mixtures and found that a solution of 70% of cold ethanol gave slightly better results than those obtained with the other mixtures (Fig. 1B).

Densitometry analysis of the gel showed that the cold-ethanol fraction contains mostly I20 monomer, and only trace amounts of I20-*b*-PI (lane 2, Fig. 1B). Finally, the purified fraction contained 89% of I20-*b*-PI, and 11% of I20 monomers and dimers (lane 3, Fig. 1B). Despite our efforts to improve the purification process, this was the best result we could obtained.

Finally, we evaluated the solubility of the I20-*b*-PI in different organic solvents (Table S1†). Beside the chloroform/methanol 4 : 1 mixture, the copolymer was soluble in DMF, in DMF/THF 1 : 4 mixture, and to a lower extent in DCM.

Characterization of I20-*b*-PI

Purified I20-*b*-PI was first analyzed by size exclusion chromatography in DMF (Fig. 2A). The chromatogram obtained with the non-reduced I20 sample, containing a mixture of monomers and dimers, showed two peaks. The larger one representing 75% of the sample corresponds to the I20 monomers, and the smaller one corresponds to the I20 dimers. Their molar mass calculated by comparison with polystyrene standards were respectively 10 and 23 kg mol^{-1}. The SEC trace for the purified I20-*b*-PI revealed one main peak with a retention time intermediate between those of the I20 monomers and dimers, and a calculated molar mass of 16.5 kg mol^{-1} ($Đ$ = 1.1). A small shoulder can be noticed at low retention times corresponding most probably to some I20-*b*-PI dimers (34 kg mol^{-1}). It should be noted that the proportion of these dimers were lower after SDS-PAGE analysis (see lanes 3 Fig. 1A and B), strongly suggesting that they are formed by non-covalent intermolecular bonds, such as hydrophobic inter-chain interactions mediated by the PI moiety.

I20, PIMAL, and purified I20-*b*-PI were analyzed by infrared spectroscopy (Fig. 2B).

After the coupling reaction, the stretching vibration of –CH_3 (2960 cm^{-1}) and –CH_2– (2914 cm^{-1}, 2853 cm^{-1}) of PI were detected in the I20-*b*-PI compound. In addition, the reaction between the thiol function of I20 and the double bond of

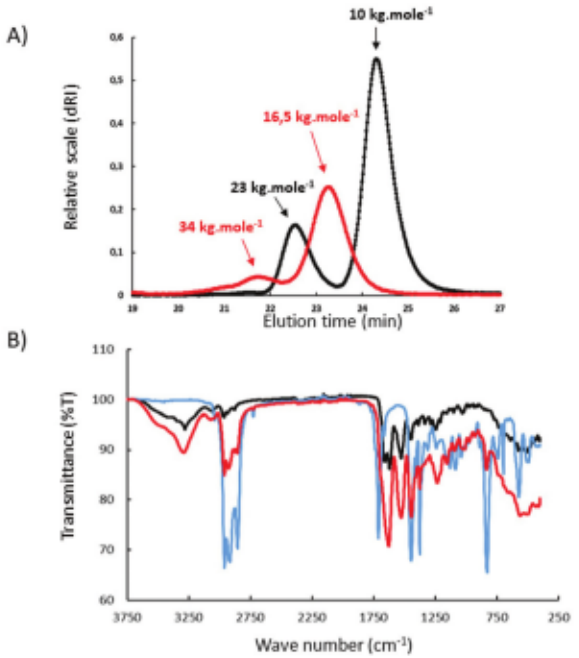

Fig. 2 (A) SEC traces of I20 and I20-*b*-PI using a RI detector. I20-*b*-PI (red line) and I20 (black line) were dissolved in DMF at a concentration of 5 mg mL^{-1}, and then filtrated through 0.45 μm PTFE filters. 40 μL solution was injected into the column at 40 °C. (B) Infrared spectra of ELP I20, PIMAL and I20-*b*-PI. 1 mg of dried I20, PIMAL and purified I20-*b*-PI were analyzed at room temperature by infrared with a Bruker VERTEX 70. The corresponding traces of I20 (black), PIMAL (blue) and I20-*b*-PI (red) were superimposed for comparison.

PIMAL led to a shift of the stretching vibration of ketone to 1628 cm^{-1}, and to the disappearance of the bending vibration of –C–H *cis* double bond from maleimide. Altogether, these results strongly suggest that the reaction took place between the thiol function of the I20 cysteine, and the double bond of the maleimide. This result was confirmed by NMR analyses. Correlation between carbon and proton signals were obtained from the ^{1}H–^{13}C heteronuclear single quantum correlation (HSQC) of I20-*b*-PI copolymer (Fig. 3). It can be observed cross-peaks corresponding to the I20 part (green) and to the PIMAL part (red). First, it must be noticed the total disappearance of the signal due to the protons of the double bond from maleimide of the PIMAL compound (Fig. S5, 14 and 15†) showing a quantitative conversion. Moreover, the reaction between the thiol function of I20 and the double bond of PIMAL led to the appearance of new peaks corresponding to the pyrrillidine-2,4-dione moiety. The crosspeaks in blue at (a) δ 2.71/26.6 ppm, (b) δ 3.24/49.6 ppm, (c) δ 2.49/34.1 ppm, (d) 4.31/65.0 ppm were assigned to the link between maleimide of PIMAL and cysteine of I20. Heteronuclear multiple bond correlation (HMBC) spectroscopy involves proton–carbon connectivities through coupling over two or three bonds and is valuable for the peak assignments of non-protonated carbons, such as carbonyl carbons.

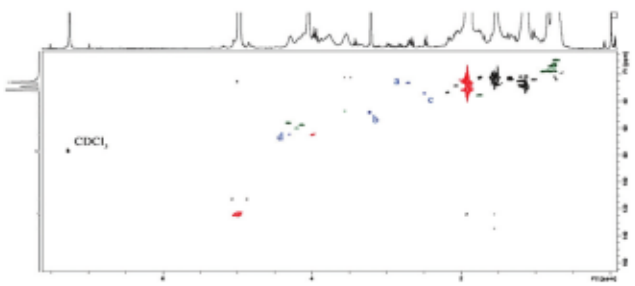

Fig. 3 2D HSQC NMR spectra of I20-*b*-PI showing the correlation between the two blocks in $CDCl_3$.

I20-*b*-PI self-assembly in aqueous solvent

We chose the nanoprecipitation technique to obtain I20-*b*-PI nanoparticles. Briefly, purified diblocks were solubilized in DMF/THF solution at a concentration of 2 mg mL^{-1}, and then water was added drop by drop to form the nanoparticles. After extensive dialysis to remove the organic solvent, the resistance of the nanoparticles to dilution was tested by serial dilution. The critical aggregation concentration (CAC) of the copolymer was measured by a fluorometric method using pyrene as the fluorophore[26] (Fig. 4A).

The CAC value was calculated to be 50 μg mL^{-1}, which corresponds to a molar concentration of 3.5 μM. This low CAC

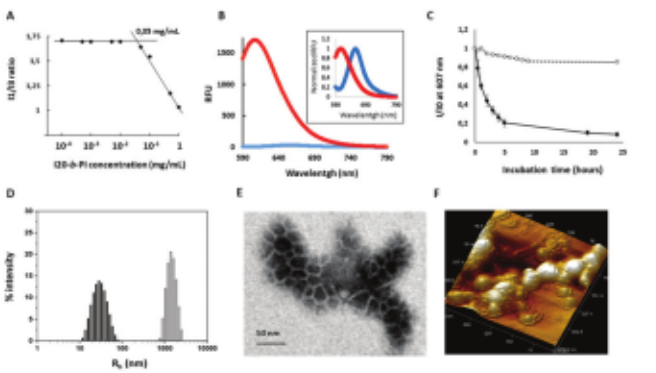

Fig. 4 Characterization of ELP-*b*-PI nanoparticles. (A) CAC measurement of I20-*b*-PI. CAC was calculated by measuring the ratio of the fluorescence intensities of pyrene (10 μM) measured at 373 nm and 385 nm. This ratio was plotted against the I20-*b*-PI concentration to calculate the CAC. (B) Encapsulation of the lipophilic stain Nile red. Fluorescence of a Nile red solution in water (blue), and with I20-*b*-PI nanoparticles (red). Relative data to the maximal value of each sample are shown in the inset. (C). Fluorescence of the Nile red *versus* time. 1 mL of Nile red-loaded particles (0.27 mg mL^{-1}) were placed in a dialysis device and incubated in 1 L of water at 20 °C. The emission of fluorescence at 607 nm was measured at different time points. Data are mean of three independent experiments ± SD (●). As a control the fluorescence of a suspension of Nile red-loaded particles at same concentration (0.27 mg mL^{-1}) was monitored during 24 h (○). (D) DLS analysis of particles obtained by nanoprecipitation of I20-*b*-PI. Black bars represent the result obtained in water. Grey bars represent the result obtained in PBS. (E) TEM images of I20-*b*-PI nanoparticles. (F) AFM images of I20-*b*-PI nanoparticles. 3-D projection of particles combining height and phase channels.

value can be explained by the presence of the very hydrophobic PI moiety in the copolymer, in agreement with previous studies which showed that both the sizes of the hydrophobic block, and the hydrophilic/hydrophobic ratio influence the CAC value.[27,28] Indeed, the CAC value measured for I20-*b*-PI is in the same range (3–5 μM) as that measured for ELP-C14 diblocks.[28] The capacity of the nanoparticles to encapsulate the lipophilic stain Nile red was also evaluated. I20-*b*-PI nanoparticles in water were incubated for 24 h with a Nile red solution, and the fluorescence of the sample was measured (Fig. 4B). When incubated in water, Nile red was barely fluorescent, with 32 relative fluorescence units (RFU) at its maximal wavelength emission of 654 nm. After incubation with I20-*b*-PI nanoparticles, the fluorescence intensity increased dramatically to 1710 RFU. In addition, the maximal wavelength emission shifted from 654 nm to 607 nm in the presence of the nanoparticles (inset Fig. 4B) demonstrating that the dye was in a hydrophobic environment.[29] This experiment shows that the I20-*b*-PI nanoparticles can efficiently load a hydrophobic molecule. Nile red release was studied by placing the loaded nanoparticles into a dialysis device, and by measuring the fluorescence at 607 nm at different times (Fig. 4C). We measured a 40% decrease in the fluorescence intensity during the first hour, and then a slower decrease. After 5 h and 24 h of dialysis, the fluorescence intensity of the samples was respectively 20% and 8% of the initial value. To control that this decrease in fluorescence was not due either to bleaching of Nile red or to nanoparticles dissociation during the experiment, we also incubated a suspension of Nile red-loaded I20-*b*-PI nanoparticles for 24 h without dialysis. We showed that under this condition the decrease in fluorescence was low, with more than 91% of the initial fluorescence intensity remaining after 5 h of incubation, and still 85% of the initial fluorescence intensity after 24 h. Altogether, these data show that a hydrophobic drug can be efficiently released from the I20-*b*-PI nanoparticles.

The hydrodynamic radius of the particles obtained after nanoprecipitation was measured by DLS. A typical result is shown in Fig. 4D. Independent experiments were performed with four different batches of I20-*b*-PI. The mean R_h of the particles was 39.4 ± 4.9 nm, and the PDI was 0.132 ± 0.011. Stability of these nanoparticles was first evaluated by incubating them for up to 46 days at 4 °C (Table S2†). This experiment showed a slight increase in the PDI value during the first day up to 0.24, but then this index, as well as the scattered intensity of the sample did not change substantially for 46 days suggesting that no significant aggregation took place. Next, we studied the behavior of the nanoparticles upon heating treatment. Indeed, the ELP moiety of the diblock has a T_t around 19 °C,[16,17] and we wanted to see if heating the nanoparticles will change their size. The size of the nanoparticles did not significantly vary between 10 and 60 °C; the DCR and PDI remained constants as well indicating that no significant aggregation took place (Fig. S13†). These results strongly suggest that the intrinsic thermosensitivity of I20 did not have a significant influence on the I20-*b*-PI nanoparticles formation and stability. To explain this result, we can raise two hypotheses. The first one is that the hydrophobicity of the PI moiety is so important, that this is the main driving force in the self-association of the nanoparticles, and consequently the thermosensitivity of I20 became negligible. In other words, the fact that the ELP shell was totally hydrated (below its T_t), or partially dehydrated (above its T_t) neither changed the nanoparticle dimensions nor their propensity to self-aggregate, at least at the concentrations used. The second hypothesis is that after the coupling reaction and the different successive steps of washing and drying, the ELP corona was not totally soluble in water at a temperature below its T_t, and consequently the intrinsic thermosensitivity of the ELP was lost. To investigate further we performed circular dichroism (CD) analyses of the ELP and I20-*b*-PI samples (Fig. S14†). Indeed, numerous studies have shown that the thermosensitivity of ELPs is the consequence of conformational changes between the soluble and aggregated state.[30–32] This is the case for the ELP I20, with a large negative peak around 235 nm at 15 °C which can be ascribed to β-turns.[33] This peak disappeared after heating at 30 °C. This confirms that the secondary structure of I20 differs in its soluble and aggregated form. Different results were obtained for I20-*b*-PI. At low temperature, we did not observe a large negative peak around 235 nm. In addition, no significant changes were observed upon heating, only a small decrease in ellipticity in the 190–230 nm region. Finally, the spectra obtained for I20-*b*-PI were highly similar to that of I20 at 30 °C. From these results, we can conclude that the grafting of one molecule of PI at the C-terminal end of I20 led to a conformational change, and that the corresponding secondary structure is similar to that adopted when the unmodified ELP is incubated at a temperature above its T_t. This explains our previous observation that the size of the I20-*b*-PI nanoparticles did not change when we varied the temperature.

To understand the stability of the nanoparticles in water, we measured their surface charge. Zeta value was measured to be around −33 mV (Fig. S15†). This negative value explains why the nanoparticles are quite stable when stored in water. However, the presence of negative charges at the surface of the nanoparticles is not straightforward. Indeed, I20 which is exposed at the surface of the nanoparticles, does not contain any negatively-charged amino acid in its sequence, only neutral ones. The only charge might come from the N-terminal amine, and therefore would be expected to be a positive one. However, the average pK_a of the N-terminal amine of proteins is generally in the 7–8 range,[34] and therefore this group should not be significantly charged in water solution. An explanation for the negative Zeta value of hydrophobic materials has already been made. Indeed, it has been previously demonstrated that when an hydrophobic material is placed in water, the OH^- ions which are present in solution bind to the interface of the material, and therefore this layer of negatively charged ions provides a negative charge on the particle surface.[35]

Finally, we evaluated the stability of the nanoparticles in PBS buffer, which is more biologically relevant than pure

water. Results of the DLS measurement are shown in Fig. 4D. PBS addition to the solution containing the nanoparticles immediately triggered their aggregation in particles of about 1200 nm. As shown previously, the I20-*b*-PI nanoparticles are negatively charged in water, owing to the presence of an OH^- layer at their surface. When salts are added, this negative layer of hydroxide ions is screened, and the hydrophobic nanoparticles start to aggregate. Of course, we will have to take this phenomenon into account if we want to find a biomedical application to our nanoparticles.

The morphology of the I20-*b*-PI nanoparticles was also observed by TEM (Fig. 4E and Fig S16†) and AFM (Fig. 4F). Particles ranging between 20 and 30 nm in radius can be seen with the two techniques. The particles were aggregated as a consequence of the dehydration process during sample preparation. TEM images show particles constituted by a black core, most probably made of the PI block which is more stained by osmium because of its reactivity with the double bonds, surrounded by a clearer ring made of the ELP block that has a low electron density.

Two biomedical applications could be foreseen for this material. The first one is the possibility to obtain hydrophobic drug depot after injection into human tissues. After encapsulation of a hydrophobic drug into the I20-*b*-PI particles, and injection into the human body, the saline concentration of serum will trigger their rapid aggregation at the subcutaneous or intramuscular injection site. This will lead to the formation of a drug depot which will gradually release the encapsulate drug, which could be an anticancer drug, a hydrophobic antibiotic or even an antigen for immunization purpose.[36–39] The second application would be to use this rubber-based material in tissue repair strategies. Indeed, such material could be used to replace specific rubbery tissues such as intervertebral discs.[40] However, this will require the synthesis of larger amounts of I20-*b*-PI, and therefore to scale-up the synthesis and purification process.

Conclusions

In this work, we successfully coupled poly(1,4-*cis*-isoprene) and an elastin-like polypeptide. This bio-based diblock was characterized by different physico-chemical techniques. Particles of 30–45 nm of R_h were obtained by nanoprecipitation in water, and it was shown that they could encapsulate and release a hydrophobic dye.

Author contributions

The manuscript was written through contributions of all authors. TZ achieved all the synthesis and most of the self-assembly experiments. FP and BG conceptualized the study. NMR analysis were performed and interpreted by ALW, microscopy analysis and interpretation by EI, interpretation of DLS by CS. FR performed the CD experiments and interpreted the results. All authors have given approval to the final version of the manuscript.

Conflicts of interest

There are no conflicts to declare.

Acknowledgements

We acknowledge the China Scholarship Council and Université de Bordeaux (UB-CSC 2018) for the financial support of TZ. CNRS, Univ. Bordeaux and Bordeaux INP are acknowledged for their financial support. The microscopy was carried out in the Bordeaux Imaging Center, a service unit of the CNRS-INSERM and Bordeaux University, member of the national infrastructure France BioImaging. The authors thank Amélie Vax for the help with SEC measurements, Tim Delas for DLS analyzes, Martin Fauquignon and Pablo Gomez Argudo for CAC measurements. The authors would like to thank Sébastien Lecommandoux for fruitful discussions.

Notes and references

1 M. Morell and J. Puiggalí, *Polymers*, 2013, **5**, 188–224.
2 T. Deming, H.-A. Klok and H. Schlaad, in *Advances in Polymer Science*, ed. H.-A. Klok and H. Schlaad, Springer-Verlag, Berlin/Heidelberg, 2006, vol. 202, pp. 1–18.
3 J. Yunyongwattanakorn, Y. Tanaka, S. Kawahara, W. Klinklai and J. Sakdapipanich, *Rubber Chem. Technol.*, 2003, **76**, 1228–1240.
4 S. Amnuaypornsri, J. Sakdapipanich, S. Toki, B. S. Hsiao, N. Ichikawa and Y. Tanaka, in *Rubber Chemistry and Technology*, Rubber Division of the American Chemical Society, 2008, vol. 81, pp. 753–766.
5 Y. Tanaka, *Prog. Polym. Sci.*, 1989, **14**, 339–371.
6 S. Sato, Y. Honda, M. Kuwahara and T. Watanabe, *Biomacromolecules*, 2003, **4**, 321–329.
7 R. Yoda, Y. Hirokawa and T. Hayashi, *Eur. Polym. J.*, 1994, **30**, 1397–1401.
8 A. V. Radchenko, J. Grange, A. Vax, F. Jean-Baptiste-Dit-Dominique, R. Matmour, S. Grelier and F. Peruch, *Polym. Chem.*, 2019, **10**, 2456–2468.
9 J. Rodríguez-Hernández, J. Babin, B. Zappone and S. Lecommandoux, *Biomacromolecules*, 2005, **6**, 2213–2220.
10 D. W. Urry, T. L. Trapane and K. U. Prasad, *Biopolymers*, 1985, **24**, 2345–2356.
11 D. W. Urry, *Prog. Biophys. Mol. Biol.*, 1992, **57**, 23–57.
12 B. Li, D. O. Alonso and V. Daggett, *J. Mol. Biol.*, 2001, **305**, 581–592.
13 D. E. Meyer and A. Chilkoti, *Biomacromolecules*, 2004, **5**, 846–851.
14 E. Garanger and S. Lecommandoux, *Angew. Chem., Int. Ed.*, 2012, **51**, 3060–3062.
15 J. Kyte and R. F. Doolittle, *J. Mol. Biol.*, 1982, **157**, 105–132.

16 L. Bataille, W. Dieryck, A. Hocquellet, C. Cabanne, K. Bathany, S. Lecommandoux, B. Garbay and E. Garanger, *Protein Expression Purif.*, 2015, **110**, 165–171.
17 L. Bataille, W. Dieryck, A. Hocquellet, C. Cabanne, K. Bathany, S. Lecommandoux, B. Garbay and E. Garanger, *Protein Expression Purif.*, 2016, **121**, 81–87.
18 D. E. Meyer and A. Chilkoti, *Nat. Biotechnol.*, 1999, **17**, 1112–1115.
19 A. Mohr, P. Talbiersky, H. G. Korth, R. Sustmann, R. Boese, D. Bläser and H. Rehage, *J. Phys. Chem. B*, 2007, **111**, 12985–12992.
20 L. Piñeiro, M. Novo and W. Al-Soufi, *Adv. Colloid Interface Sci.*, 2015, **215**, 1–12.
21 S. Gillier-Ritoit, D. Reyx, I. Campistron, A. Laguerre and R. Pal Singh, *J. Appl. Polym. Sci.*, 2003, **87**, 42–46.
22 J. Folch-Pi and P. J. Stoffyn, *Ann. N. Y. Acad. Sci.*, 1972, **195**, 86–107.
23 M. B. Lees, *Neurochem. Res.*, 1998, **23**, 261–271.
24 M. B. Folch and J. Lees, *J. Biol. Chem.*, 1951, **191**, 807–817.
25 M. S. Bahniuk, A. K. Alshememry, S. V. Elgersma and L. D. Unsworth, *J. Nanobiotechnol.*, 2018, **16**, 15.
26 J. Aguiar, P. Carpena, J. A. Molina-Bolívar and C. Carnero Ruiz, *J. Colloid Interface Sci.*, 2003, **258**, 116–122.
27 M. Bagheri, J. Bresseleers, A. Varela-Moreira, O. Sandre, S. A. Meeuwissen, R. M. Schiffelers, J. M. Metselaar, C. F. Van Nostrum, J. C. M. Van Hest and W. E. Hennink, *Langmuir*, 2018, **34**, 15495–15506.
28 K. M. Luginbuhl, D. Mozhdehi, M. Dzuricky, P. Yousefpour, F. C. Huang, N. R. Mayne, K. L. Buehne and A. Chilkoti, *Angew. Chem., Int. Ed.*, 2017, **56**, 13979–13984.
29 R. Plenderleith, T. Swift and S. Rimmer, *RSC Adv.*, 2014, **4**, 50932–50937.
30 T. Yamaoka, T. Tamura, Y. Seto, T. Tada, S. Kunugi and D. A. Tirrell, *Biomacromolecules*, 2003, **4**, 1680–1685.
31 S. M. Janib, M. F. Pastuszka, S. Aluri, Z. Folchman-Wagner, P. Y. Hsueh, P. Shi, Y. A. Lin, H. Cui, J. A. MacKay, P. S. Conti, Z. Li and J. A. MacKay, *Polym. Chem.*, 2014, **5**, 1614–1625.
32 F. G. Quiroz and A. Chilkoti, *Nat. Mater.*, 2015, **14**, 1164–1171.
33 A. Micsonai, F. Wien, L. Kernya, Y.-H. Lee, Y. Goto, M. Réfrégiers and J. Kardos, *Proc. Natl. Acad. Sci. U. S. A.*, 2015, **112**, E3095–E3103.
34 G. R. Grimsley, J. M. Scholtz and C. N. Pace, *Protein Sci.*, 2009, **18**, 247–251.
35 C. S. Tian and Y. R. Shen, *Proc. Natl. Acad. Sci. U. S. A.*, 2009, **106**, 15148–15153.
36 H. Betre, W. Liu, M. R. Zalutsky, A. Chilkoti, V. B. Kraus and L. A. Setton, *J. Controlled Release*, 2006, **115**, 175–182.
37 W. Wang, A. Jashnani, S. R. Aluri, J. A. Gustafson, P. Y. Hsueh, F. Yarber, R. L. McKown, G. W. Laurie, S. F. Hamm-Alvarez and J. A. MacKay, *J. Controlled Release*, 2015, **199**, 156–167.
38 C. A. Gilroy, M. E. Capozzi, A. K. Varanko, J. Tong, D. A. D'Alessio, J. E. Campbell and A. Chilkoti, *Sci. Adv.*, 2020, **6**, eaaz9890.
39 D. Asai, T. Fukuda, K. Morokuma, D. Funamoto, Y. Yamaguchi, T. Mori, Y. Katayama, K. Shibayama and H. Nakashima, *Macromol. Biosci.*, 2019, **19**, 1900167.
40 R. D. Bowles and L. A. Setton, *Biomaterials*, 2017, **129**, 54–67.